Bulletin of the Seismological Society of America, Vol. 93, No. 1, pp. 94–108, February 2003

Multiple Seismogenic Processes for High-Frequency Earthquakes at Katmai National Park, Alaska: Evidence from Stress Tensor Inversions of Fault-Plane Solutions

by Seth C. Moran

Abstract The volcanological significance of seismicity within Katmai National Park has been debated since the first seismograph was installed in 1963, in part because Katmai seismicity consists almost entirely of high-frequency earthquakes that can be caused by a wide range of processes. I investigate this issue by determining 140 well-constrained first-motion fault-plane solutions for shallow (depth $<$ 9 km) earthquakes occurring between 1995 and 2001 and inverting these solutions for the stress tensor in different regions within the park. Earthquakes removed by several kilometers from the volcanic axis occur in a stress field characterized by horizontally oriented σ_1 and σ_3 axes, with σ_1 rotated slightly (12°) relative to the NUVEL1A subduction vector, indicating that these earthquakes are occurring in response to regional tectonic forces. On the other hand, stress tensors for earthquake clusters beneath several Katmai cluster volcanoes have vertically oriented σ_1 axes, indicating that these events are occurring in response to local, not regional, processes. At Martin-Mageik, vertically oriented σ_1 is most consistent with failure under edifice loading conditions in conjunction with localized pore pressure increases associated with hydrothermal circulation cells. At Trident-Novarupta, it is consistent with a number of possible models, including occurrence along fractures formed during the 1912 eruption that now serve as horizontal conduits for migrating fluids and/or volatiles from nearby degassing and cooling magma bodies. At Mount Katmai, it is most consistent with continued seismicity along ring-fracture systems created in the 1912 eruption, perhaps enhanced by circulating hydrothermal fluids and/or seepage from the caldera-filling lake.

Introduction

High-frequency earthquakes are perhaps the most enigmatic type of seismic event to occur in association with volcanoes. On the one hand, we understand fairly well what a high-frequency earthquake (defined as a seismic event with significant high-frequency content and impulsive *P* and/or *S* arrivals [e.g., Malone, 1983; Lahr *et al.*, 1994]) represents: the brittle fracture of rock along a fault plane. On the other hand, a wide variety of processes can cause high-frequency earthquakes to occur, including tectonism, hydrofracturing, gravitational loading and failure, thermal and volumetric forces associated with magma intrusion, withdrawal, and/or cooling, or some combination of any or all of these. One way that volcano seismologists have attempted to address this issue has been to make a distinction between high-frequency earthquakes caused by tectonic forces ("tectonic" earthquakes [e.g., Malone, 1983; Klein *et al.*, 1987]) and those related to volcanic processes ("volcano-tectonic," or VT, earthquakes [e.g., Latter, 1981; Malone, 1983; Klein *et al.*, 1987; Lahr *et al.*, 1994]). This distinction is made largely on the qualitative basis of the closeness of a given high-frequency earthquake to a volcanic vent (Malone, 1983; Klein *et al.*, 1987).

The notion that high-frequency earthquakes can be caused by a wide range of processes is illustrated by recent studies of background seismicity at Mounts Rainier and St. Helens in Washington State. Moran (1994) and Giampiccolo *et al.* (1999) demonstrated that post-1986 background VT earthquakes at Mount St. Helens are likely occurring in response to periodic intrusions of new magma into the volcanic plumbing system. However, Moran *et al.* (2000) showed that background VT earthquakes at Mount Rainier are likely occurring in response to a combination of gravitational loading and localized pore-pressure increases caused by fluids derived from cooling magma bodies at depth. In addition, earthquakes located just ~15 km to the west of Mount Rainier were found by Giampiccolo *et al.* (1999) and

Moran *et al.* (1999) to be most simply explained by regional tectonic forces and thus are considered to be tectonic earthquakes. These and other studies of high-frequency earthquakes occurring in volcanic areas (e.g., Jolly *et al.*, 1994; De Natale *et al.*, 2000; Sanchez, 2000; Roman *et al.*, 2001; Legrand *et al.*, 2002) demonstrate that many different processes in volcanic environments can cause this type of seismic event. Thus it is problematic to assume *a priori* a cause for high-frequency earthquakes occurring in volcanic environments without using constraints from earthquake characteristics and other geophysical and geological studies to narrow down the range of possible causes. These studies also demonstrate that high-frequency earthquakes are a potentially rich source of information about ongoing volcanic processes, even when volcanoes are inactive.

In this article I attempt to constrain the source processes responsible for high-frequency earthquakes occurring in association with the Katmai volcanic cluster, located in Katmai National Park, Alaska (Fig. 1). In 1912 the Katmai volcanic cluster was the site of the most voluminous eruption of the twentieth century, when ~13 km^3 (dense rock equivalent) of magma was erupted over a period of ~60 hr (Fierstein and Hildreth, 1992). The Katmai area continues to be one of the most seismically active volcanic areas in Alaska, with a yearly average of 852 located earthquakes that consist almost exclusively of high-frequency earthquakes. Many of these are spatially associated with volcanic centers, but others are removed by several kilometers from the nearest center (Fig. 2), and questions about their volcanological significance have been raised since the first seismometers were deployed in the park in 1963 (Decker, 1963). I address these questions by computing fault-plane solutions for 140 earthquakes occurring between 1995 and 2001 and inverting these fault-plane solutions for stress tensors in spatially segregated earthquake clusters, including those beneath Mounts Martin and Mageik, Trident and Novarupta, Mount Katmai, and north and east of Snowy Mountain (Fig. 2). The resulting stress tensors show that the stress field in which earthquakes occur varies significantly throughout the park. I use these results in conjunction with seismicity characteristics and constraints from other geological and geophysical studies to propose that some earthquake clusters are occurring primarily in response to tectonic forces, but that others are occurring directly or indirectly in response to volcanic processes.

Background

Eight andesite-to-dacite volcanic centers constitute the Katmai volcanic cluster within Katmai National Park. The volcanic piles are constructed on a basement of flat-lying, relatively undisturbed Mesozoic sediments of the Naknek formation (Wallmann *et al.*, 1990). In map-view the many vents in the cluster form a remarkably straight segment trending N66°E from Mount Martin to Snowy Mountain (Fig. 1). Only Novarupta and Mount Griggs are located behind (relative to the trench) this segment. Trident, Novarupta, and Mount Katmai all erupted in the twentieth century, and Mounts Martin, Mageik, and Griggs and Snowy Mountain have all been active in the Holocene (Hildreth and Fierstein, 2000; Fierstein and Hildreth, 2001). The most recent eruptions issued from a new vent, now known as Southwest Trident (Hildreth and Fierstein, 2000), on the southwest flank of Trident between 1953 and 1974. They consisted of a series of andesite lava flows and minor explosive activity (Hildreth and Fierstein, 2000). A recent interferometric synthetic aperture radar (InSAR) study of the Trident area by Lu *et al.* (1997) found that several centimeters of uplift had occurred between 1993 and 1995 around the vent, which they determined was the result of inflation of a Mogi-type source at 0.8–2.0 km depth. Fumaroles emanate from Griggs, Katmai, Mageik, Martin, Novarupta, Snowy, and Trident (Wood and Kienle, 1990; Hildreth and Fierstein, 2000), providing further evidence of ongoing magmatic activity.

The relatively high level of volcanic activity is matched by a high rate of seismicity. The first earthquakes known to have occurred in the Katmai area were in association with the 1912 eruption. Abe (1992) was able to use recordings of these events on undamped Milne seismographs from Victoria, British Columbia, Honolulu, Hawaii, and elsewhere to positively identify 50 events as occurring in association with this eruption, with magnitudes ranging from 4.8 to 7.0. The cumulative seismic moment associated with these events is an order of magnitude larger than that associated with other twentieth century caldera-forming eruptions, including Fernandina in 1968 and Pinatubo in 1991 (Filson *et al.*, 1973; Mori *et al.*, 1996; Hildreth and Fierstein, 2000).

The first indication of a post-1912 high seismicity rate came from a temporary seismograph that recorded 82 earthquakes over a 17-day period in 1963 (Decker, 1963). A subsequent three-station network installed in 1965 recorded 1800 local earthquakes in 39 days, the majority of which had depths less than 10 km (Matumoto and Ward, 1967). This included a 1-day-long swarm of VT events located in the vicinity of Snowy Mountain. Several other similar networks were operated on a temporary basis through the next 2 decades (e.g., Matumoto, 1971; Pulpan and Kienle, 1979). The first extensive seismic network was installed in Katmai during 1987–1988 and, at its peak, consisted of 14 short-period seismometers, including five three-component instruments (Ward *et al.*, 1991). Nineteen hundred hypocenters were calculated for events occurring between September 1987 and December 1990, or ~580 events per year. Although this rate is significantly less than that reported by Matumoto and Ward (1967), this number includes only those events for which locations could be determined, whereas the 1965 rate is based purely on event counts. Unfortunately, the data recorded by this network is not readily available at this time (A. M. Pitt, personal comm., 2001), and thus cannot be included in this article.

The seismic network currently operating in Katmai was

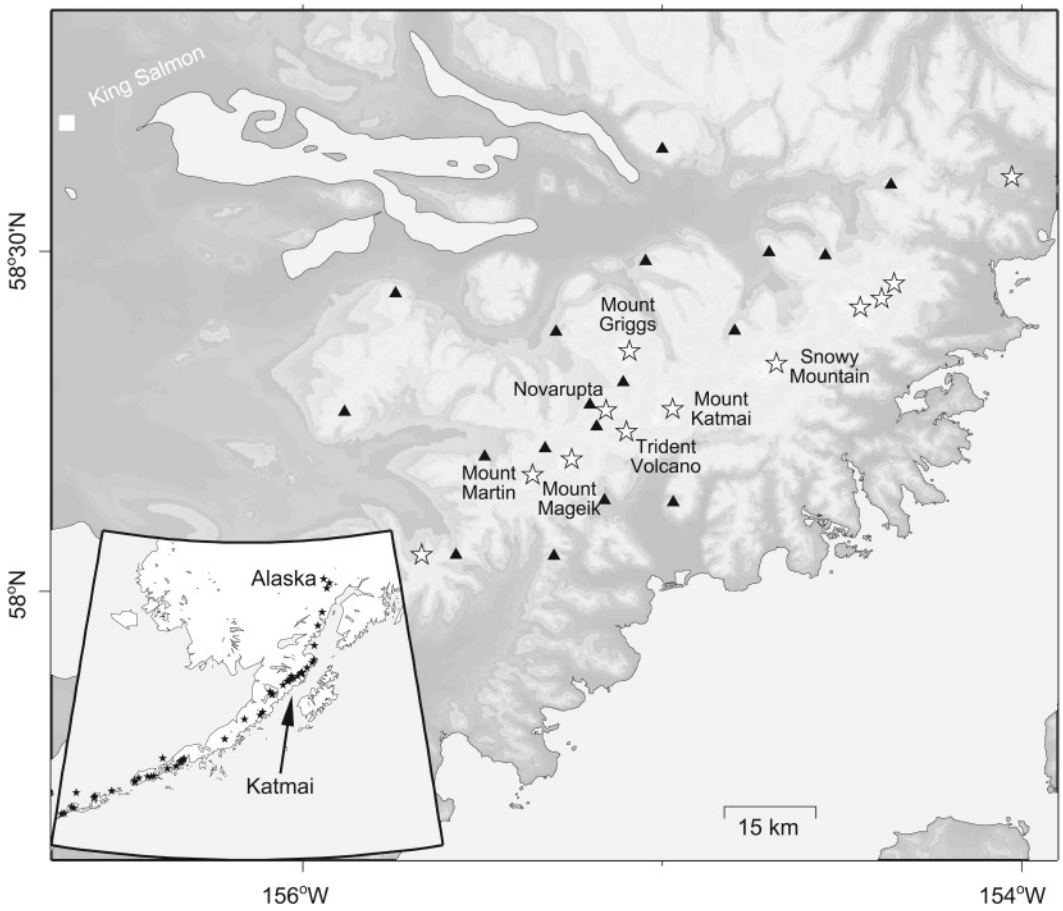

Figure 1. Map showing location of volcanoes in Katmai National Park (stars) and AVO seismograph stations (triangles). Inset map indicates location of Katmai on the Alaska Peninsula, with stars indicating locations of volcanic centers active in the Holocene.

installed by the Alaska Volcano Observatory (AVO) in three stages during the summers of 1995 (five stations), 1996 (six stations), and 1998 (seven stations) (Jolly *et al.*, 2001). The full network consists of 18 stations (Fig. 1) and 24 components. The initial five stations were reoccupied from the Ward *et al.* (1991) network and hence have the same names (see Figure 1 in Ward *et al.* [1991]). Seismometers at 15 of these sites are Mark Products L4-C 1-Hz vertical components, and the 3 other sites have Mark Products L22 2-Hz three-component seismometers. Signals from these sites are telemetered in real time via line-of-sight radio transmission to King Salmon (Fig. 1), where they are placed on commercial phone circuits and sent to AVO operational centers in Fairbanks and Anchorage. The signals are then digitized at 100 samples/sec, analyzed by both automated processes and manually (locations, counts, etc.), and archived in both continuous and segmented formats (Jolly *et al.*, 2001).

Seismicity, 1995–2001

Since its installation in July 1995, the AVO seismic network in Katmai National Park has recorded 5518 locatable earthquakes within the park through the end of 2001 (Fig. 2), roughly 30% of all earthquakes located for all volcanoes monitored by AVO during this time period. I relocated 3494 of these events in the 3D velocity model computed by Jolly (2000). Figure 3 shows the 1736 well-constrained relocated hypocenters, including only those that were recorded on at least six stations and had azimuthal gaps less than 180° and a nearest station within 20 km. The average formal epicentral and hypocentral errors for the relocated hypocenters are 0.66 and 1.33 km, respectively. Only nine of these hypocenters have depths greater than 8 km below sea level, and the vast majority have depths less than 5 km (Fig. 3).

Of all 5518 located events, only 8 were classified by AVO analysts as long-period (LP) earthquakes (e.g., Lahr *et al.*, 1994). Of these, five were shallow (depths <4 km) and three were deep (depths >20 km). Six additional deep LP events have been identified through subsequent detailed analyses (J. Power, personal comm., 2002). All other located earthquakes within the park are either tectonic or VT earthquakes. Table 1 shows the total number of earthquakes per year located by AVO in the Katmai area. The yearly total has declined somewhat steadily since a peak of 1334 in

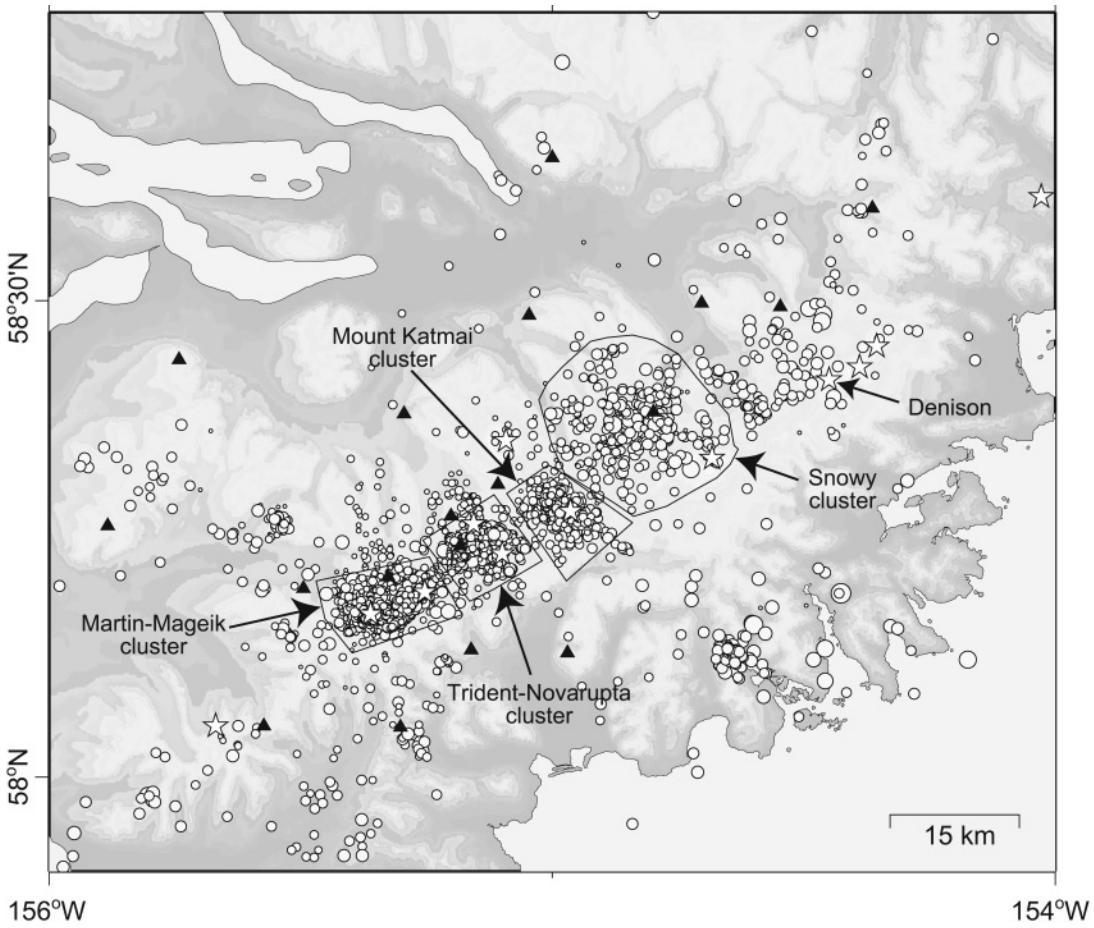

Figure 2. Map showing all earthquakes (light gray circles) located by AVO between 1995 and 2001 with at least six phase arrivals. Locations of four earthquake clusters are indicated by boxes and labeled; see text for descriptions. Average epicentral and hypocentral errors are 2.5 and 8.5 km, respectively. Black triangles correspond to seismograph stations, and white stars to volcanic centers.

1996, despite yearly increases in the number of seismic stations through 1998. It is interesting to note that the average rate of 515 earthquakes per year in 2000–2001 is comparable to the 1987–1990 rate recorded by Ward *et al.* (1991) on their similar-sized network, suggesting that seismicity rates in 1996–1998 were elevated. The magnitude of completeness (M_c) is 0.7 for all Katmai earthquakes occurring between 1995 and 2001, with a *b*-value of ~1 (the M_c value for the Ward *et al.* [1991] network is unknown). However, Jolly and McNutt (1999) found that values of M_c changed depending on station availability and location and also found significant spatial and temporal heterogeneity in *b*-values between 1995 and 1997.

As can be seen in Figures 2 and 3, the majority of these earthquakes are spatially clustered, with most clusters occurring beneath, or near, several volcanoes in the Katmai Group (e.g., Ward *et al.*, 1991; Jolly and McNutt, 1999). Distinct clusters are located beneath Mounts Martin and Mageik (referred to here as the Martin-Mageik [MM] cluster), between Trident and Novarupta (the Trident-Novarupta [TN] cluster), and beneath Mount Katmai. East of Mount Katmai seismicity abruptly becomes more diffuse, with spatially ill-defined clusters occurring NNE of Snowy Mountain and west of Denison (Fig. 2). There are also scattered earthquakes along the volcanic axis that are not associated with these clusters, as well as earthquakes that occur in other areas of the park that are not spatially close to any volcanic center. Apparent seismicity clusters also occur outside the Katmai seismic network, including one west and north of Dennison and another south of the axis along the Pacific coast. Because these clusters fall outside of the network, however, the locations for events in the clusters are poorly constrained, and thus these clusters are not considered here. Roughly 56% of all located Katmai earthquakes lie within the MM cluster, 20% in the TN cluster, 10% beneath Mount Katmai, 8% in the diffuse Snowy cluster, and 6% elsewhere within the park (Table 2). In cross section there is an apparent increase in maximum hypocentral depths from west-southwest to east-northeast (Fig. 3b), perhaps reflecting a gradual deepening of the brittle-ductile transition along the volcanic axis.

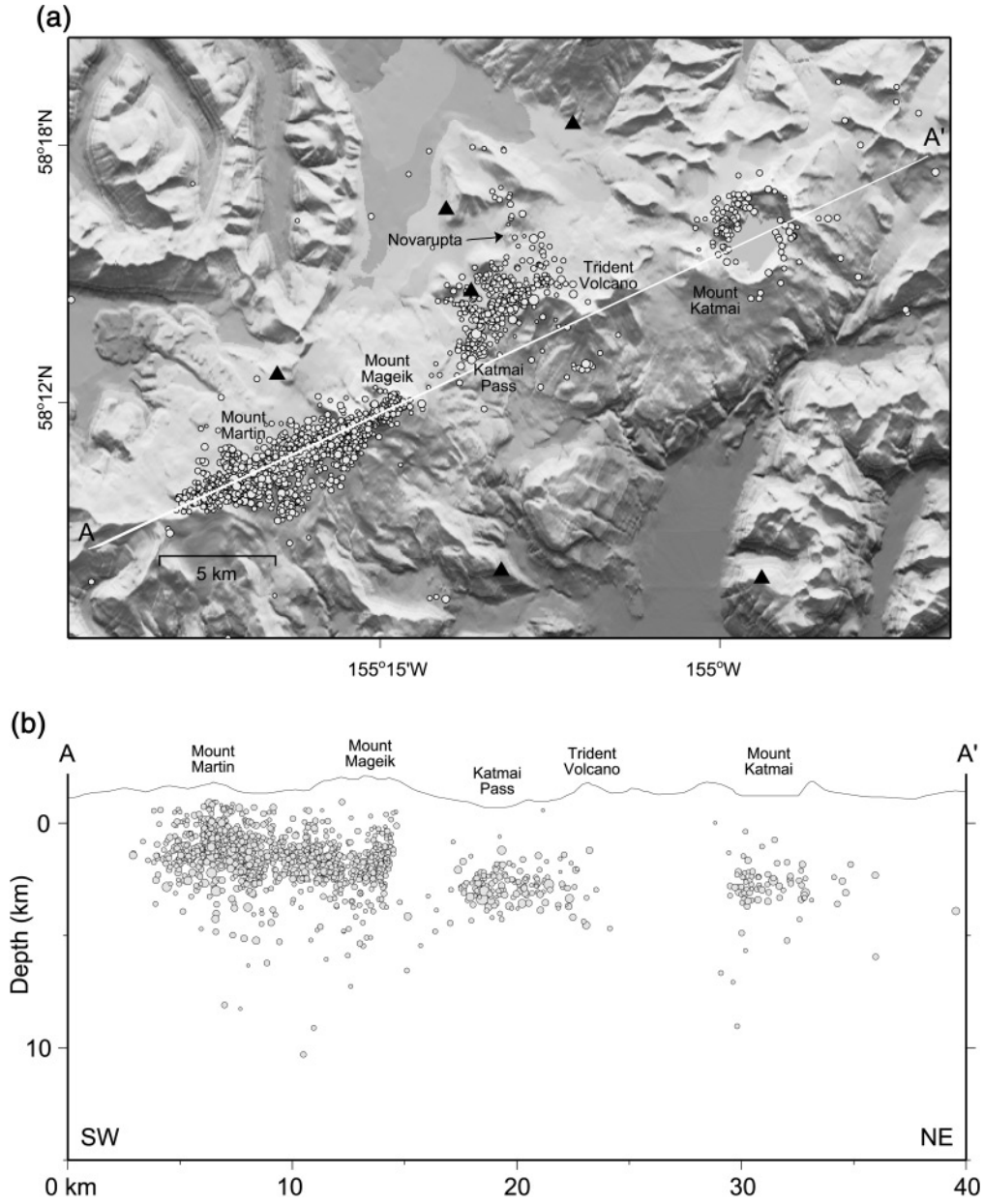

Figure 3. (a) Shaded relief map of the Katmai volcanic cluster with well-constrained hypocenters (at least 7 *P* arrivals, gap <180°, nearest station <15 km) relocated using the 3D velocity model of Jolly (2000) and the methodology of Moran *et al.* (1999). Most hypocenters in the Martin-Mageik cluster are located between the two edifices, those for the Trident-Novarupta cluster are located west and north of the Trident edifice, and virtually all hypocenters in the Mount Katmai cluster are located either beneath the northwestern or southeastern rims of the lake-filled caldera. The white line labeled A-A′ drawn along the volcanic axis corresponds to the cross-sectional profile shown in Fig. 3b. (b) Southwest-northeast cross section showing relocated hypocenters within 5 km of A-A′ profile (oriented N66°E; see Fig. 3a). There is no vertical exaggeration. Note that, in general, maximum hypocentral depths appear to increase to the northeast (toward A′), and the vast majority of earthquakes are located above 5 km depth, suggesting a shallow brittle-ductile transition. Zero kilometers corresponds to sea level.

Table 1
Number of Earthquakes Located in the Katmai Area per Year by AVO

Year	No. of Located Earthquakes	No. of Installed Stations	Comments
1995	297	5	Five stations installed 07/95
1996	1334	11	Six stations installed 07/96; swarm at Mageik 10/96
1997	947	11	
1998	950	18	Seven new stations on-line 09/98
1999	959	18	
2000	500	18	
2001	531	18	

Table 2
Number of Earthquakes Located within Five Katmai Seismicity Groups

Cluster/Group	No. of Located Earthquakes	Maximum Magnitude (M_L)
Martin-Mageik	3078	2.9
Trident-Novarupta	1126	4.5
Mount Katmai	543	3.5
Snowy Mountain	419	3.6
Other events	352	3.8

The spatial distribution of 1995–2001 epicenters is virtually identical to the distribution of 1987–1990 epicenters (compare Fig. 2 with figure 1 from Ward *et al.* [1991]), indicating that earthquakes are occurring in response to processes that can be regarded as relatively steady state over a 15-yr time period. However, superimposed upon this are occasional earthquake swarms, including a 1-day-long swarm near Snowy in 1965, inferred to be a typical volcanic earthquake swarm by Matumoto and Ward (1967), and a 10-day-long swarm of over 450 located VT earthquakes beneath the Mageik edifice in 1996, inferred by Jolly and McNutt (1999) to be a result of an actively degassing intrusion emplaced at some depth below the maximum depth of seismicity. There have been several instances of small earthquake swarms occurring simultaneously at Martin, Mageik, Trident, and Mount Katmai that were apparently triggered by several nearby $M_w > 6.5$ earthquakes (Power *et al.*, 2001; Moran *et al.*, 2001).

In addition to days-to-weeks-long swarms, there are also fluctuations in seismicity rates over months-to-years timescales, particularly at Martin and Mageik. Table 2 shows that seismicity rates were significantly higher during 1996–1999 than in 2000–2001, and Figure 4 shows that most of this drop is attributable to a marked (~67%) decrease in MM seismicity rates between 1999 and 2000. This drop is likely not an artifact of network outages (a not inconsequential consideration in locations like Katmai with extreme climatic conditions), as the number and duration of station outages were roughly equivalent during these two time periods (Jolly *et al.*, 2001). Also, seismicity rates in other clusters showed either no decline or much smaller declines, indicating that the detection threshold of the Katmai network has remained roughly the same on a year-to-year basis since it was completed in 1998.

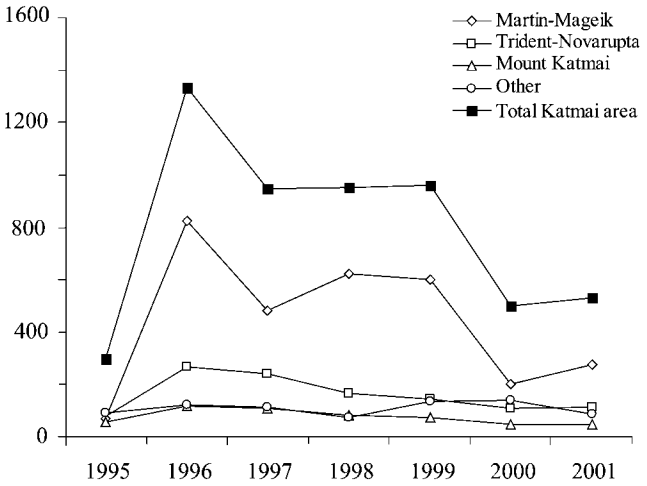

Figure 4. Chart comparing the yearly number of located earthquakes in each cluster and the whole park from 1995 to 2001. Note that the seismic network only operated for ~5 months in 1995 and that the network increased in size in 1996 and 1998 (Jolly *et al.*, 2001). Note also that the ~50% drop in located earthquakes between 1999 and 2000 is due almost exclusively to a seismicity decline in the MM cluster.

Previous investigators have used regional and teleseismic travel-time delays (Ward *et al.*, 1991), *S*-wave shadows (Matumoto and Ward, 1967; Matumoto, 1971), *b*-values and swarm characteristics (Matumoto and Ward, 1967; Jolly and McNutt, 1999), and local earthquake *P*-wave velocity and attenuation tomography (Jolly, 2000) to look for evidence of magma bodies and to infer causes for the earthquake clusters. Matumoto and Ward (1967) provided perhaps the best summary statement to date for all Katmai earthquakes when they ascribed them to "a mixture of tectonic and volcanic shocks in a highly heterogeneous structure with locally concentrated stresses."

Stress-Tensor Inversion

Data

The initial steps in my analysis were to reanalyze individual earthquakes, add or remove first motions where appropriate, and compute fault-plane solutions (FPSs). Only those hypocenters with maximum station-azimuthal gaps less than 180°, magnitudes greater than 1.0, at least one station within 20 km of the epicenter, and maximum formal location errors of less than 5 km were considered. Large teleseisms and regional events were used to establish whether individual stations had reversed polarities and, if so, over what time span (Table 3). FPSs were then computed

Table 3
History of Reversed Polarities on Katmai Network Stations

Station	Time Span of Station Reversal
ACH	1999/07/16–present
KAPH	1998/10/12–present
KCG	1995/07/26–1996/07/25
KCG	1997/07/20–present
KEL	1995/07/26–1997/07/20
KVT	1995/07/26–1997/07/20

using the program FPFIT (Reasenberg and Oppenheimer, 1985).

FPFIT implicitly assumes that all events are double couple. This assumption has been shown by several investigators to be incorrect in specific regions, including geothermal and volcanic areas (e.g., Julian and Sipkin, 1985; Julian *et al.*, 1997; Miller *et al.*, 1998). However, since there are only three three-component stations in the Katmai network, there is insufficient waveform data to perform moment tensor inversions or other waveform analyses to investigate whether or not Katmai VT events are double couple. Additionally, the number of first motions for even the largest events is too small to be able to uniquely determine whether or not any FPS is truly non-double-couple. Since the first-motion distributions for all events analyzed are consistent with the double-couple assumption made by FPFIT, I feel that the double-couple assumption is a reasonable one to make at Katmai.

FPSs for 191 events with at least seven first motions were initially computed. All FPSs with misfits greater than 0.15, station distribution ratios (a factor sensitive to the distribution of polarities relative to nodal planes [Reasenberg and Oppenheimer, 1985]) less than 0.4, and/or averaged uncertainties in the strike, dip, and rake of the solution greater than 40° were discarded. In addition, all FPSs were carefully inspected to ensure that first motions were well distributed across the focal sphere with no polarity discrepancies that could have a significant effect on the FPS. Individual events with multiple FPSs were rejected if the multiple FPSs were significantly different and equally plausible (indicating that no nonunique solution existed); otherwise, the best of the multiple FPSs was chosen and all others discarded. These selection criteria yielded 140 well-constrained FPSs (Fig. 5), generally for those events with $M_L > 1.3$. The average formal epicentral and hypocentral errors for all 140 events are 0.7 and 1.6 km, respectively. Since FPSs can be sensitive to changes in depth, I recomputed FPSs from each cluster using depths that varied by ± 1 km. Although changes were observed in some cases, the overall sense of each FPS (i.e., normal, reverse, or strike-slip) was invariant to changes in depth.

All types of mechanisms are represented in this dataset, although pure thrust mechanisms are vastly outnumbered by normal and strike-slip mechanisms. In general, normal mechanisms tend to occur preferentially beneath the volcanic centers, whereas strike-slip and oblique-slip mechanisms tend to dominate in the off-axis areas (Fig. 5).

Stress Field Analysis

The spatial variability of FPSs in Figure 5 suggests that the stress field in the Katmai area is spatially heterogeneous. To test this hypothesis I used the focal mechanism stress inversion (FMSI) computer programs of Gephart and Forsyth (1984) and Gephart (1990) to invert for the best-fitting stress tensor in different volumes. In this method a grid search is performed over a range of stress tensors, using the minimum amount of rotation about any axis required to bring the slip direction into alignment with the resolved shear stress on a fault plane as the measure of misfit (Φ). The smallest Φ of the two candidate fault planes in each FPS is chosen and summed with the smallest Φs for all other solutions and averaged to give an average Φ for the whole dataset. An individual stress field is described by the dip and azimuth of the three principal stress directions (σ_1, σ_2, σ_3) and R, a measure of the relative magnitudes of the three principal stresses [where $R = (\sigma_2 - \sigma_1)/(\sigma_3 - \sigma_1)$]. This method assumes that stress is uniform throughout the volume considered, that earthquakes occur on pre-existing faults, and that slip occurs in the direction of the resolved shear stress on a fault plane. The misfit Φ has been shown by several investigators to be an indicator of the degree of stress-field heterogeneity in a given volume. In particular, Wyss *et al.* (1992) showed that values of $\Phi < 6°$ were reflective of a homogeneous stress field, whereas values of $\Phi > 9°$ were reflective of a heterogeneous stress field. In this article I consider values of $\Phi > 6°$ as evidence that a particular volume has a spatially or temporally heterogeneous stress field.

For a given Φ, confidence intervals are computed using the methods described by Parker and McNutt (1980) and Gephart and Forsyth (1984). The sizes of these intervals are influenced by the number of FPSs in a particular dataset (fewer = larger intervals, particularly for datasets with fewer than 20 FPSs), as well as the degree of stress field heterogeneity (e.g., Giampiccolo *et al.*, 1999). However, Hardebeck and Hauksson (2001) have demonstrated that confidence regions for the Gephart and Forsyth (1984) method are in most cases too large. Thus I view the intervals shown in Figure 6 to be conservative.

For each population of FPSs I performed an initial inversion using a 10-degree grid and the exact method of FMSI. I used the orientation of σ_1 from the NUVEL1A model ($\sigma_1 = 337°$ in the Katmai area; DeMets *et al.*, 1990) as a starting stress model for all inversions ($\sigma_1 = 337°$, $\sigma_3 = 67°$, dips = 0°, variance = 90°). Other starting models were tested, but the final results did not vary significantly from this starting model. I used the best-fitting model from the initial inversion as a starting model for the next inversion, which was performed using the exact method of FMSI and a 5-degree grid. Subsequent iterations were performed in a similar fashion until no appreciable improvement in misfit

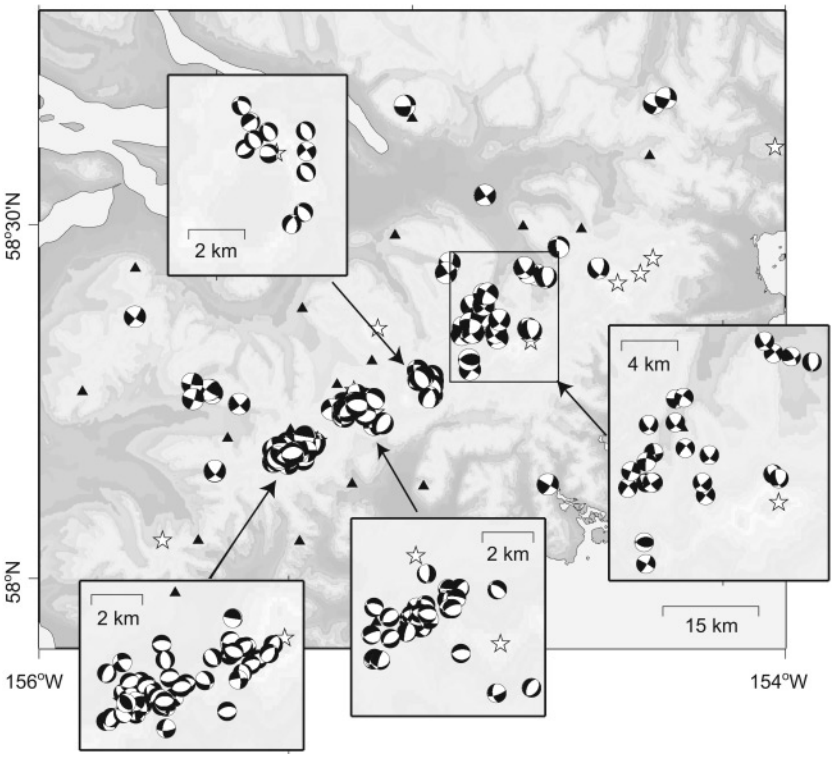

Figure 5. Map showing all 140 fault-plane solutions calculated for the Katmai area between 1995 and 2001. Other symbols are as in Figures 1 and 2.

was achieved, at which point I considered the inversion to have converged.

I initially inverted all 140 FPSs and found that the best-fitting model had a large misfit (8.27°) and was also significantly different from the assumed stress model for the regional tectonic stress field (Table 4). The large misfit indicates that the stress field in the Katmai area is either spatially or temporally heterogeneous (or both). To investigate temporal heterogeneity I used the cumulative misfit method of Lu and Wyss (1996) with a variety of stress models. I found no significant variations over time, as might have been expected given the quasi-steady-state nature of seismicity over the 1987–2001 time period. I then subdivided the FPSs into five groups based on the spatial clustering of hypocenters (Figs. 2 and 3). These clusters included the MM, TN, Mount Katmai (MK), and Snowy clusters, and those events occurring at a distance from the volcanic axis (hereafter referred to as the "off-axis" group). The best-fitting stress tensors for each of these regions are listed in Table 4, and plots with 90% confidence intervals are shown in Figure 6.

Discussion

Tectonic Versus VT Events

One of the most obvious trends to emerge from this analysis is the near-horizontal orientations for both σ_1 and σ_3 in the off-axis and "off-axis + Snowy" (or OAS) group, in contrast to the vertical orientation of σ_1 in the MM, TN, and MK clusters. Inversions were also performed for the off-axis and Snowy groups independently (Table 4), but the low misfit of 4.53° from inversion of the combined populations indicates that the OAS group is fairly homogeneous with respect to the stress tensor and thus further subdivision is not quantitatively justified. The azimuthal orientation of σ_1 (349°) in the OAS group is fairly close to the NUVEL1A model for the subduction vector ($\sigma_1 = 337°$). It is also subparallel to the direction of maximum horizontal stress inferred by Nakamura *et al.* (1980) for the eastern Aleutian are based on orientations of linear chains of cinder cones on the flanks of major volcanoes, as well as to the ~160° orientation of the dominant joint set found in the TN area by Wallmann *et al.* (1990). These observations provide strong support for the hypothesis that the earthquakes in these two groups are occurring primarily in response to tectonic forces and should therefore be regarded as tectonic, not VT, earthquakes. If true, then the stress tensor for the OAS group provides one of the first seismically derived estimates of the orientation of the regional stress field in the upper crust in the Katmai area, as well as along most of the Alaskan Peninsula. Although the subduction vector falls just outside the 90% confidence limit for the OAS group (Fig. 6), the difference is small enough to be inconclusive in terms of evidence for any rotation of the regional stress field that might be expected as a result of "escape tectonics" associated with the collision of the Yakutat terrane in south-central Alaska (Haeussler *et al.*, 2000).

Vertical Orientation of σ_1

Although there is considerable overlap in possible stress tensors within the 90% confidence interval for the MM, TN,

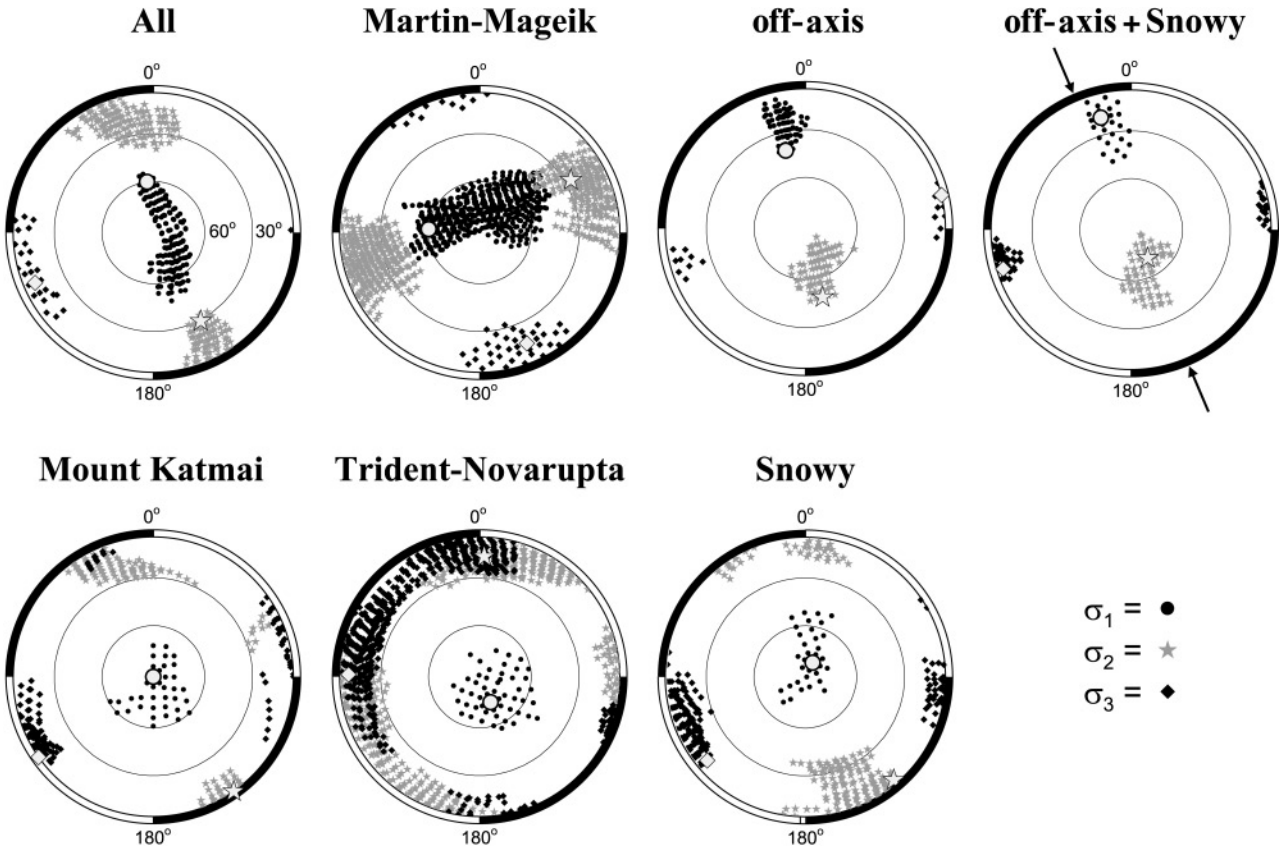

Figure 6. Stereo plots showing the best-fitting stress tensors and stress tensors with misfits less than the 90% confidence interval determined in stress-tensor inversions of different spatial groupings of fault-plane solutions (see Tables 4 and 5 for details of best-fitting stress tensors). Small black circles correspond to orientations of σ_1, gray stars to orientations of σ_2, and black diamonds to orientations of σ_3; large open circle/star/diamond corresponds to axis orientations for best-fitting stress tensor. Arrows in the off-axis + Snowy plot correspond to the NUVEL1A subduction vector in the Katmai area.

Table 4
Best-Fitting Stress Tensors for Katmai Subgroups

Group	No. FPS	Misfit Φ	σ_1 az	σ_1 dip	σ_2 az	σ_2 dip	σ_3 az	σ_3 dip	R
All	140	8.27°	16°	76°	155°	11°	247°	9°	0.4
Martin/Mageik	56	8.64°	44°	60°	259°	25°	162°	15°	0.4
Trident/Novarupta	30	5.75°	92°	71°	197°	5°	289°	19°	0.6
Mount Katmai	11	2.04°	92°	83°	330°	3°	239°	5°	0.4
Snowy	19	3.93°	22°	81°	149°	5°	239°	7°	0.3
off-axis +	22	3.39°	349°	19°	142°	69°	256°	9°	0.5
off-axis + Snowy	41	4.53°	349°	31°	173°	58°	80°	2°	0.4

and MK subgroups, the vertical orientation of σ_1 is robust. This orientation is significantly different from the regional stress field inferred from either the OAS stress tensor or the NUVEL1A model. This indicates that events in these subgroups are occurring in response to stresses generated primarily by local, not regional, processes, and are therefore referred to here as VT events.

Vertical orientations for σ_1 (reflective of normal faulting) are not uncommon in volcanic areas (e.g., Jolly *et al.*, 1994; Giampiccolo *et al.*, 1999; Moran *et al.*, 2000; Sanchez, 2000) and in mountainous regions (e.g., Zoback, 1992). There are several possible interpretations for the significance of vertically oriented σ_1. In mountainous regions such as the Basin and Range, normal faulting is likely related to horizontal extensional stresses induced by buoyancy (e.g., Zoback, 1992). This could also apply to volcanic regions, where doming associated with magma intrusion at depth would give rise to horizontal extensional stresses above the

intrusion (e.g., Jolly *et al.*, 1994). Crustal loading by volcanic edifices is another model invoked by several investigators (Jolly *et al.*, 1994; Moran *et al.*, 2000). De Natale *et al.* (2000) used finite element modeling to demonstrate that gravitational loading has an important effect on the local stress field around volcanoes and can produce stress concentrations that exceed the Coulomb failure criteria for strike-slip and normal faulting. Since several volumetrically large monitored volcanoes (e.g., Mounts Shasta and Adams in the Cascade Range and Mount Griggs in the Katmai cluster) are virtually aseismic, Moran *et al.* (2000) argue that other processes, such as localized increases in pore pressure and/or geochemical weakening associated with systemic hydrothermal circulation, are required in addition to crustal loading for normal faulting to occur. Another process that could lead to normal faulting is slumping above a region where magma has been withdrawn, an extreme example of which would be caldera formation (e.g., Bailey *et al.*, 1976). Such failures also occur above man-made cavities such as tunnels (e.g., Terzaghi and Richart, 1952). Finally, Moran *et al.* (2000) noted that "edifice disintegration" due to geochemical alteration of parts of the edifice could also lead to internal slumping along normal faults within volcanic edifices.

In the following three subsections I use stress tensor orientations in conjunction with geologic observations, seismicity characteristics, and other geophysical observations made within Katmai National Park to determine preferred hypotheses for explaining vertical orientations of σ_1 in each of the three subgroups.

Martin-Mageik. Topographic buoyancy, magma withdrawal, and edifice disintegration can largely be discarded as causative processes at MM. If the normal faulting were due to topographic buoyancy, then one might expect σ_3 to be oriented perpendicular to the topographic ridge defined by the Martin and Mageik edifices, with fault planes oriented parallel to the ridge. Although the best-fitting σ_3 orientation is roughly perpendicular, the high misfit (8.64°) suggests that the stress field is fairly heterogeneous. However, inversions of Martin-only and Mageik-only FPSs yielded poorly constrained stress tensors that were not significantly different from the MM tensor, and in the Martin case the misfit was even greater (9.66°; see Table 5). Closer inspection of the MM FPSs reveals that there is significant variability in fault-plane orientations (Fig. 7). This variability suggests that the causative source processes operate on a more local scale than would be expected for topographic buoyancy. In addition, topographic buoyancy would presumably result in seismicity along the entire extent of the topographic ridge, whereas MM seismicity occurs only between Martin and Mageik; the rest of the ridge west of Martin is relatively aseismic (Fig. 2).

Hypocentral patterns are the primary evidence against both edifice disintegration and edifice loading as source processes. The fact that most, if not all, VT earthquakes locate below the base of the edifice, not within it, is the best argument against edifice disintegration (Fig. 3). And, as mentioned above, almost all MM events are concentrated between the two edifices, not along the entire ridge, arguing against edifice loading alone. However, edifice loading in conjunction with other processes such as hydrothermal circulation, as proposed by Moran *et al.* (2000) for Mount Rainier, is a viable hypothesis for MM VT events. Given the 10-day swarm in 1996 attributed to a magmatic intrusion (Jolly and McNutt, 1999) and the vigorous fumaroles emanating out of both Martin and Mageik, it seems reasonable to call upon the presence of an actively degassing body (or bodies) at shallow depths below the base of seismicity. The hydrothermal system at MM is more vigorous than that at Mount Rainier, as is the seismicity rate (25 well-located earthquakes per month at MM versus 1–2 per month at Rainier [Moran *et al.*, 2000]). The combined MM edifice is much smaller, however ($\sim$30 versus $\sim$140 km^3 for Rainier). Thus gravity may be less important at MM, but hydrothermal circulation more important, suggesting that the flux of volatiles and fluids may be the factor that most strongly controls seismicity rates under edifice loading conditions. The high misfit for the best-fitting stress tensor (which indicates a high degree of heterogeneity in the stress field) fits well with this model, since a system that has multiple hydrothermal circulation cells would be expected to have highly localized stress fields.

In this context, the longer-term variations in seismicity rates shown in Table 2 and Figure 4 may be attributable to longer-term changes in volatile and/or fluid flux rates perhaps related to cyclic emplacement and cooling of small magma bodies. However, the fact that current seismicity patterns are virtually identical to those recorded by Ward *et al.* (1991) between 1987 and 1991, and arguably to those recorded by Matumoto and Ward (1967) in 1965, suggests that the cyclically intruded bodies are so small as to not signifi-

Table 5
Best-Fitting Stress Tensors for Martin/Mageik Subgroups

Group	No. FPS	Misfit Φ	σ_1 az	σ_1 dip	σ_2 az	σ_2 dip	σ_3 az	σ_3 dip	R
Martin	16	9.78°	33°	39°	278°	27°	164°	39°	0.1
Remainder	40	5.49°	112°	76°	270°	13°	1°	5°	0.6
Mageik	16	4.42°	6°	77°	263°	3°	173°	13°	0.5
Remainder − Mageik	24	5.42°	274°	63°	60°	23°	156°	13°	0.3

az, azimuth.

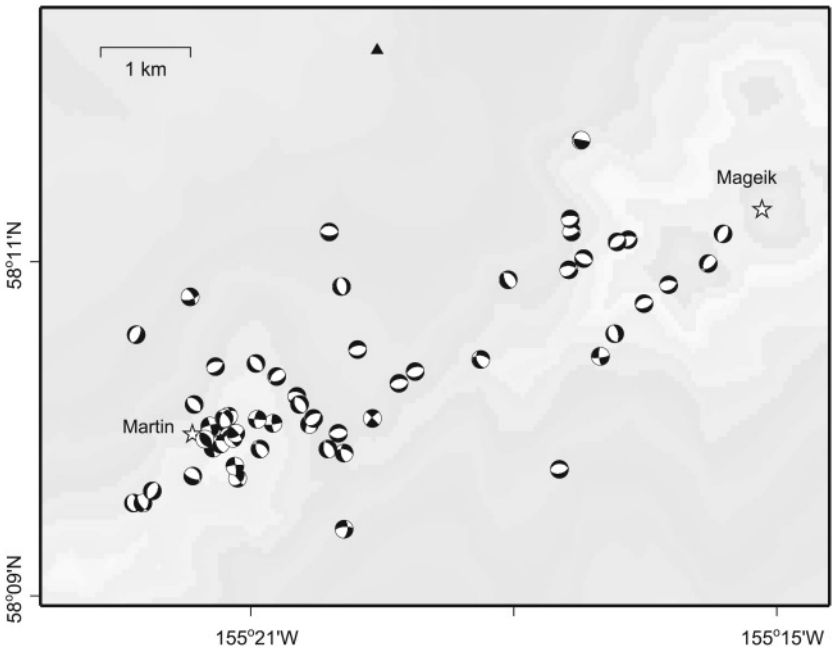

Figure 7. FPSs from the MM cluster. Note the much greater diversity in types of FPSs directly beneath Martin, indicating that the stress field near the Martin vent may be spatially distinct from the rest of the MM cluster.

cantly change the plumbing system beneath either edifice. This is also borne out by the fact that the location and vigor of fumaroles at both Martin and Mageik have been relatively unchanged since they were first photographed in 1913–1917 (Fierstein and Hildreth, 2001).

Trident-Novarupta. The VT events at TN appear to be occurring in response to different source processes than those at MM. This is suggested in part by differences in the inverted stress tensor for TN, which also has a vertical orientation for σ_1 but a significantly smaller misfit (5.75° versus 8.64°) than the MM stress tensor, indicating that the TN stress field is more homogeneous. A distinct source process is also suggested by differences in seismicity characteristics. The *b*-values at TN ($b \sim 1.0$) are significantly lower than at MM (Jolly and McNutt, 1999; Jolly, 2000), indicating lower geothermal gradients (Warren and Latham, 1970), higher applied shear stress (Scholz, 1968), higher effective stress (or lower pore pressures; Wyss, 1973), and/or a lower degree of material heterogeneity (Mogi, 1962) at TN relative to MM. Lower geothermal gradients are also indicated by the slightly greater maximum depths of TN events (Fig. 3), suggesting a slightly deeper brittle-ductile transition. Higher applied and/or effective stresses are indicated by the fact that the two largest earthquakes ever recorded by AVO in Katmai occurred within this cluster, an M_L 4.5 and an M_L 3.9 on 1 April 1997.

Further evidence suggesting a different source process for TN earthquakes lies in their hypocentral locations, the vast majority of which are not beneath the Trident edifice. Instead, many occur in an area of minimal topography bounded by the Mageik edifice to the west, the several dacite domes (including Novarupta) to the north and west, and the four Trident stratocones to the south and east (Fig. 3). Thus topographic loading is not a significant factor for most of the TN seismicity. There is also less direct evidence at the surface for extensive hydrothermal circulation, as the only fumarolic activity in the TN area is found on the SE flank of Trident (on the opposite side of the seismicity) as well as at several weaker vents near the summit of Trident and Novarupta (Fierstein and Hildreth, 2001). These observations argue that the edifice loading/hydrothermal circulation hypothesis invoked for MM seismicity is problematic for TN, and thus that other local processes are likely responsible for the vertical orientation of σ_1 at TN.

One important set of constraints on the possible causes of TN seismicity comes from geophysical anomalies detected in the Trident–Katmai Pass area. Jolly (2000) found a *P*-wave low-velocity anomaly at shallow depths (0–4 km) in the Katmai Pass area, with most of the TN VT events locating along the northern margin of this anomaly (Fig. 8). Coincident with this velocity anomaly is a region of high seismic attenuations (Ward *et al.*, 1991; Jolly, 2000) and a significant Bouguer gravity low centered in the Katmai Pass area (Saltus *et al.*, 1991; Ward *et al.*, 1991) (Fig. 8). Saltus *et al.* (1991) inferred from their gravity data that a 280-km^3 magma body lies beneath Katmai Pass extending from 1 to 9 km depths. Ward *et al.* (1991) suggested that the attenuation and gravity anomalies represent geophysical signatures of the shallow magmatic system that fed the 1912 eruptions at Novarupta. The low-velocity anomaly from Jolly (2000) provides further support for the presence of at least some partial melt residing at shallow depths beneath Katmai Pass and the western flank of Trident.

The close spatial association between these anomalies and the TN earthquakes (Fig. 8) suggests a genetic relationship. However, ongoing intrusion of new magma can be ruled out as the primary cause based on the steady seismicity

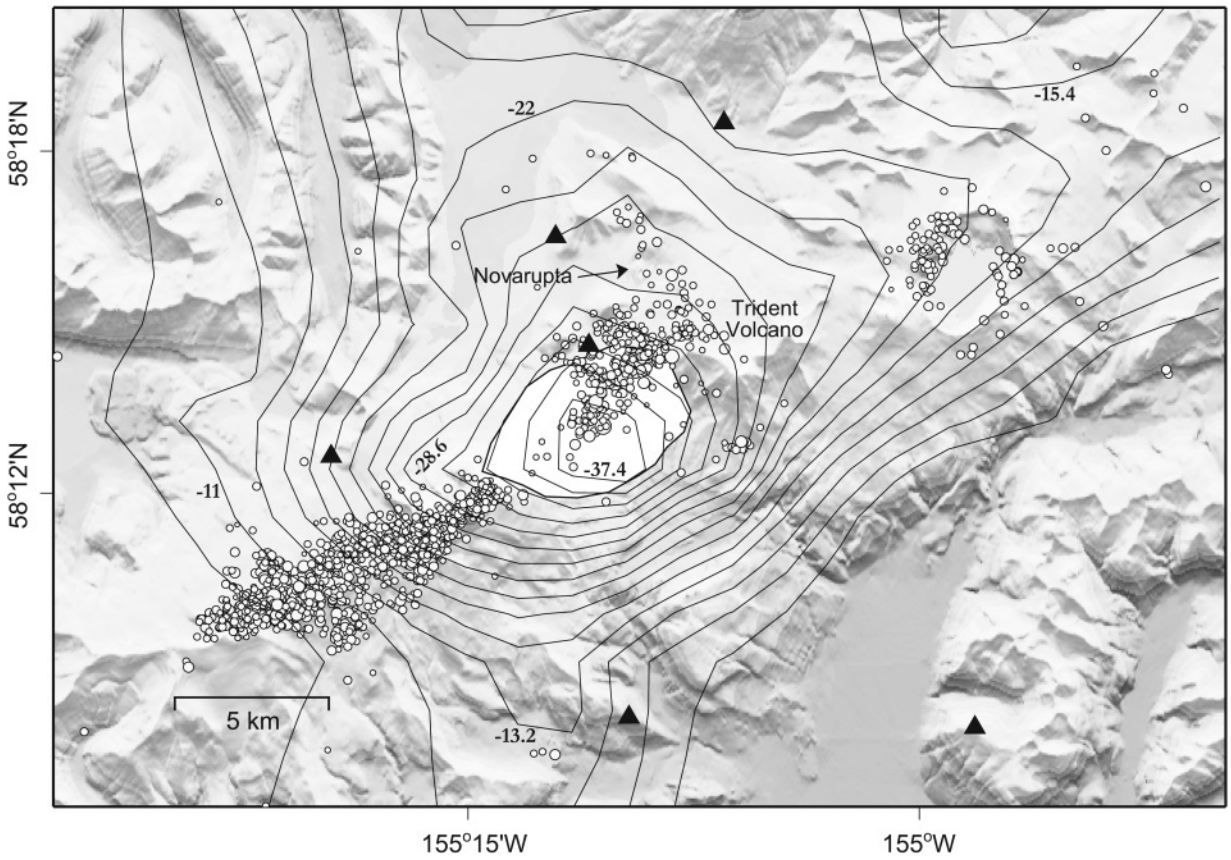

Figure 8. Map showing the relationship between well-constrained hypocenters located in the Jolly (2000) 3D velocity model (light gray circles), complete Bouguer gravity (contoured in black lines at intervals of 2.2 mGal) from Saltus *et al.* (1991) (data reduction is described in Saltus [1992]), and a region of low *P*-wave velocities ($V_p < 4.5$ km/sec; white polygon) in layer 2 (0.1–2 km) of the velocity model from Jolly (2000). Note that the TN hypocenters occur only in the north-northeastern quadrant of both anomalies, while also extending several kilometers beyond the anomaly margins to Novarupta. This pattern may indicate that they are occurring along a fault system possibly created during the 1912 eruption that connects possible small magma bodies located within the anomalies to the Novarupta vent. The map shows the same area as Figure 3a; see Fig. 3a for locations of additional geographic features.

rate (Fig. 4) and the lack of any evidence for deformation in the TN area except for the several centimeters of inflation of the SW flank of Trident, where virtually no earthquakes occur, that was detected via InSAR between 1993 and 1995 (Lu *et al.*, 1997). Unlike MM, the TN area is an excellent candidate for the application of InSAR, as there are extensive areas that retain coherency over a several-year time frame (Z. Lu, personal comm., 2001), and no definitive signs of deformation have been seen by subsequent InSAR studies since 1995 (J. Freymueller, personal comm., 2002). Additional deformation information comes from electronic distance meter and Global Positioning System (GPS) surveys of benchmarks established around Novarupta in 1990 (Kleinman *et al.*, 1995) and Trident in 1997 (J. Freymueller, personal comm., 2002). Kleinman *et al.* (1995) found movement at two of the Novarupta benchmarks due either to a deformation source southeast of the network or to benchmark instability. Campaign GPS surveys in 1998 and 2000 found evidence only for localized subsidence at the SW Trident vent (J. Freymueller, personal comm., 2002). Thus there is little surficial evidence of magmatic movement in the TN area, particularly where most of the TN seismicity has been occurring since 1987.

One possibility is that TN seismicity is a result of interactions between cooling and degassing bodies of magma in the Katmai Pass area and the surrounding country rock. The nature of these interactions, however, is unclear. No heat flow study has been undertaken in the Katmai Pass area, but the relatively low *b*-values do not support a high thermal gradient, which might be expected if magma bodies were truly within a kilometer or two of the TN earthquakes. The lack of significant fumarolic activity at the surface is also counter to what would be expected for a shallow actively degassing magma body. The predominance of normal fault-

ing is also problematic. Without significant edifice loading, the most likely means for generating normal faulting is through localized bowing upward or downward of the crust in association with tectonic loading, magma intrusion, or magma withdrawal, for which there is no surficial evidence in the form of active deformation or relatively young fractures. Thus if there are magma bodies within the velocity, attenuation, and gravity anomalies centered at Katmai Pass, they are likely not very big and also probably have been there for some time (decades to centuries). Otherwise, geothermal gradients and/or fluid flux rates would presumably be much greater (as they are at Martin and Mageik).

Another possible explanation for normal faulting is that the TN seismicity is occurring along fracture sets created during the 1912 eruption centered at Novarupta. The 1912 magma is thought to have come from a series of interconnected shallow magma bodies beneath Mount Katmai and Trident that were tapped and drained during the course of the eruption (e.g., Hildreth, 1987; Hildreth and Fierstein, 2000). Wallmann *et al.* (1990) noted that radial fissures south of Novarupta and dominant orientations of bedrock joint sets in the Valley of Ten Thousand Smokes are both roughly parallel to the assumed regional direction of maximum compressive stress. They use these observations as evidence to support the hypothesis that a feeder dike propagated to Novarupta from a reservoir beneath Trident in 1912 along pre-existing fractures and joints. Since the current seismicity in the TN area is located between Trident and Novarupta, it is occurring in the area through which the posited feeder dike presumably propagated. Strong evidence to support the formation of additional fracture sets in this area during the eruption comes from the extremely energetic earthquake sequence (including 14 earthquakes with $M_s \geq 6.0$) that occurred before and after the 1912 eruption (Abe, 1992). Although precise locations and fault-plane solutions are unknown for these events, the temporal relationship established by Abe (1992) between earthquakes and distinct events in the 1912 eruption sequence indicates that the vast majority of large earthquakes occurred after eruption onset at Novarupta. Thus most earthquakes were likely normal-faulting events associated with magma withdrawal from bodies stored along the volcanic axis. These eruption-created faults, if still connected to existing magma bodies in the Katmai Pass area, would form natural surfaces along which fluids could migrate and crystallize, locally increasing pore pressures enough to periodically reactivate segments of these faults.

Unfortunately, this hypothesis is not directly supported by the TN seismicity. There is no hint of faultlike structures in the TN seismicity, even when it is relocated using the 3D velocity model of Jolly (2000) or the double-difference technique of Waldhauser and Ellsworth (2000). In addition, most FPSs have fault planes oriented perpendicular to the fissures and bedrock joints of Wallmann *et al.* (1990). These fault-plane orientations could reflect a volcanic-axis-parallel set of faults formed as the 1912 magma moved from various storage units beneath Mount Katmai, Trident, and/or the Katmai Pass area to the Novarupta feeder dike, but there is no evidence other than the FPSs to support that idea. Nevertheless, the close spatial relationship between the TN seismicity and geophysical anomalies at Katmai Pass and the TN stress tensor determined in this study (Table 3) both suggest that TN earthquakes are occurring primarily in response to magmatic processes, and it is possible that the current seismicity is occurring along normal faults created in 1912 that are being reactivated by localized pore pressure increases associated with hydrothermal circulation from nearby magma.

Mount Katmai. Unlike the other subgroups discussed in this paper, there are relatively few FPSs (11) available for the MK subgroup. Hence it is premature to make any definitive statements about the nature of the MK stress field. The 90% confidence interval for the MK stress tensor (Fig. 6) illustrates the large uncertainty that results from using a small number of FPSs, in this case particularly for σ_2 and σ_3 orientations. However, the vertical orientation of σ_1 is relatively well constrained, reflecting the fact that 10 of the 11 MK FPSs have a significant normal-faulting component. This observation warrants at least a speculative explanation for the vertical orientation of σ_1 at MK.

Like the TN cluster, seismicity occurs at a steady rate beneath MK, especially relative to the MM cluster, implying a steady-state seismogenic process. The fact that the Mount Katmai edifice overlays the majority of MK seismicity indicates that edifice loading could be playing a role, although 5 km^3 of the edifice was removed in 1912 (Fierstein and Hildreth, 2001). Although fumaroles are not as vigorous at MK as they are at MM, many fumaroles were reported within MK up through 1930, when the caldera lake began to form. More recent evidence of ongoing hydrothermal activity comes from Motyka *et al.* (1993), who found elevated temperatures at depth within the lake as well as two areas of active upwelling. Thus a hydrothermal system likely exists at MK, and edifice loading in conjunction with hydrothermal circulation is a feasible explanation for the predominance of normal faulting at MK.

A modification to this hypothesis is suggested by the spatial distribution of seismicity at MK. As can be seen in Figure 8, earthquakes are preferentially located in two areas, one along the northwest rim of the caldera, the other along the southeast rim, with a gap centered directly under the caldera-filling lake. This pattern suggests that these earthquakes may be occurring along deeper-seated (depths range from 0 to 5 km) caldera-parallel fractures, perhaps a ring-fracture set created in 1912 when the MK summit collapsed as a result of magma withdrawal to form the present-day caldera. Although several FPSs have at least one fault plane that is consistent with occurrence along caldera-wall-parallel fractures, there are not enough at present to support or refute this conjecture. Thus earthquakes may arise from continued slippage along these faults, facilitated by localized pore pressure increases associated with hydrothermal circulation and/or by seepage of lake water from the bottom of the caldera,

perhaps aided as well by the gravitational load of the MK edifice.

Conclusions

Stress tensors computed using fault-plane solutions from earthquakes occurring in spatially distinct clusters in Katmai National Park show that the stress field is highly heterogeneous within the park, indicating that several different processes give rise to high-frequency earthquakes in different regions of the park. Stress tensors determined for the Snowy cluster and other areas removed from the volcanic axis have horizontally oriented σ_1 and σ_3 axes, with σ_1 rotated $\sim 12^\circ$ from the NUVEL1A subduction vector of 337°. This indicates that these events are occurring primarily in response to regional tectonic forces and are therefore tectonic, not VT, earthquakes. Stress tensors determined for VT clusters beneath Martin-Mageik, between Trident and Novarupta, and beneath Mount Katmai all have vertical σ_1 axes, suggesting that VT events are occurring in response to local processes related directly or indirectly to magmatic activity. At Martin-Mageik, a number of factors suggest that earthquakes occur primarily as a result of migration of fluids and/or volatiles from degassing bodies of magma at some unknown depth in conjunction with edifice loading. At Trident-Novarupta, the close spatial correlation between seismicity and several geophysical anomalies suggests that earthquakes are more directly related to magmatism. This interaction may be facilitated by the presence of a posited fracture set created during the 1912 eruption in association with magma intrusion and/or withdrawal, which could provide a lateral migration path for magma-derived fluids that could locally be increasing pore pressures leading to slippage. At Mount Katmai, epicentral patterns from well-constrained locations computed using the 3D velocity model of Jolly (2000) suggest that most earthquakes occur along ring-fracture systems created during magma withdrawal in 1912. In all cases, if present seismicity rates continue, sufficient data should accumulate in the next 3–5 years to enable future stress-field studies with higher spatial and/or temporal resolution in the Katmai area. Such studies may be particularly fruitful in the MM cluster, where relatively high misfits indicate higher spatial heterogeneity than is resolvable at present, and at Mount Katmai, where the small number of FPSs prohibits more than speculation about the nature of seismogenic processes.

Acknowledgments

John Paskievitch has been instrumental in installing and maintaining a first-class network, upon which this and several other seismology research projects are highly dependent, in the harsh Katmai National Park climate, as well as in arranging most field logistics. He is also acknowledged for demonstrating how to rapidly create a drain hole in the field. Scott Stihler did much of the initial processing and locating of the Katmai data and assisted in assessing reversed polarities at the 18 Katmai stations. Art Jolly graciously allowed the use of his 3D velocity model to relocate Katmai events, and Rick Saltus provided the gravity data shown in Figure 8. Reviews and suggestions by Steve McNutt, Tom Murray, John Power, Diana Roman, Charlotte Rowe, Michael Pasyanos, and an anonymous reviewer significantly improved the manuscript. Most figures were created using Generic Mapping Tools (GMT) Software (Wessel and Smith, 1991).

References

Abe, K. (1992). Seismicity of the caldera-making eruption of Mount Katmai, Alaska in 1912, *Bull. Seism. Soc. Am.* **82,** 175–191.

Bailey, R. A., G. B. Dalrymple, and M. A. Lanphere (1976). Volcanism, structure, and geochronology of Long Valley Caldera, Mono County, California, *J. Geophys. Res.* **81,** 725–744.

Decker, R. W. (1963). Proposed volcano observatory at Katmai National Monument: a preliminary study, Dartmouth College, unpublished report, 54 pp.

DeMets, C., R. G. Gordon, D. F. Argus, and S. Stein (1990). Current plate motions, *Geophys. J. Int.* **101,** 425–478.

De Natale, G., S. M. Petrazzuoli, C. Troise, F. Pingue, and P. Capuano (2000). Internal stress field at Mount Vesuvius: a model for background seismicity at a central volcano, *J. Geophys. Res.* **105,** 16,207–16,214.

Fierstein, J., and W. J. Hildreth (1992). The Plinian eruptions of 1912 at Novarupta, Katmai National Park, Alaska, *Bull. Volcanol.* **54,** 646–684.

Fierstein, J., and W. J. Hildreth (2001). Preliminary volcano-hazard assessment for the Katmai volcanic cluster, Alaska, *U.S. Geol. Surv. Open-File Rept. 00-489*.

Filson, J., T. Simkin, and L. Leu (1973). Seismicity of a caldera collapse: Galapagos Islands 1968, *J. Geophys. Res.* **78,** 8591–8622.

Gephart, J. W. (1990). Stress and the direction of slip on fault planes, *Tectonics* **9,** 845–858.

Gephart, J. W., and D. W. Forsyth (1984). An improved method for determining the regional stress tensor using earthquake focal mechanism data: application to the San Fernando earthquake sequence, *J. Geophys. Res.* **89,** 9305–9320.

Giampiccolo, E., C. Musumeci, S. D. Malone, S. Gresta, and E. Privitera (1999). Seismicity and stress-tensor inversion in the Central Washington Cascade mountains, *Bull. Seism. Soc. Am.* **89,** 811–821.

Haeussler, P. J., R. L. Bruhn, and T. L. Pratt (2000). Potential seismic hazards and tectonics of the upper Cook Inlet basin, Alaska, based on analysis of Pliocene and younger deformation, *Geol. Soc. Am. Bull.* **112,** 1414–1429.

Hardebeck, J. L., and E. Hauksson (2001). Stress orientations obtained from earthquake focal mechanisms: what are appropriate uncertainty estimates, *Bull. Seism. Soc. Am.* **91,** 250–262.

Hildreth, W. J. (1987). New perspectives on the eruption of 1912 in the Valley of Ten Thousand Smokes, Katmai National Park, Alaska, *Bull. Volcanol.* **49,** 680–693.

Hildreth, W. J., and J. Fierstein (2000). Katmai volcanic cluster and the great eruption of 1912, *Geol. Soc. Am. Bull.* **112,** 1594–1620.

Jolly, A. D. (2000). Subsurface structure of the volcanoes in Katmai National Park, Alaska, *Ph.D. Thesis*, University of Alaska, Fairbanks.

Jolly, A. D., and S. R. McNutt (1999). Seismicity at the volcanoes of Katmai National Park, Alaska: July 1995–December 1997, *J. Volcanol. Geotherm. Res.* **93,** 173–190.

Jolly, A. D., R. A. Page, and J. A. Power (1994). Seismicity and stress in the vicinity of Mount Spurr volcano, south central Alaska, *J. Geophys. Res.* **99,** 15,305–15,318.

Jolly, A. D., S. D. Stihler, J. A. Power, J. C. Lahr, J. Paskievitch, G. Tytgat, S. Estes, A. B. Lockhart, S. C. Moran, S. R. McNutt, and W. R. Hammond (2001). Catalog of earthquake hypocenters at Alaskan volcanoes: January 1, 1994 through December 31, 1999, *U.S. Geol. Surv. Open-File Rept. 01-189; http://geopubs.wr.usgs.gov/openfile/of01-189*.

Julian, B. R., and S. A. Sipkin (1985). Earthquake processes in the Long Valley Caldera area, California, *J. Geophys. Res.* **90,** 11,155–11,169.

Julian, B. R., A. D. Miller, and G. R. Foulger (1997). Non-double-couple

earthquake mechanisms at the Hengill-Grensdalur volcanic complex, southwest Iceland, *Geophys. Res. Lett.* **24,** 743–746.

Klein, F. W., R. Y. Koyanagi, J. S. Nakata, and W. R. Tanigawa (1987). The seismicity of Kilauea's magma system, in *Volcanism in Hawaii*, R. W. Decker, T. L. Wright, and P. H. Stauffer (Editors), *U.S. Geol. Surv. Profess. Pap. 1350*, 1019–1185.

Kleinman, J. W., E. Y. Iwatsubo, J. A. Power, and E. T. Endo (1995). Geodetic studies in the Novarupta area, Katmai National Park, Alaska, 1990 to 1995, in *Geologic Studies in Alaska by the U.S. Geological Survey, 1995*, J. A. Dumoulin and J. E. Grey (Editors), *U.S. Geol. Surv. Profess. Pap. 1574*, 83–93.

Lahr, J. C., B. A. Chouet, C. D. Stephens, J. A. Power, and R. A. Page (1994). Earthquake location and error analysis procedures for a volcanic sequence: application to the 1989–1990 eruptions at Redoubt volcano, Alaska, *J. Volcanol. Geotherm. Res.* **62,** 137–153.

Latter, J. H. (1981). Volcanic earthquakes, and their relationship to eruptions at Ruapehu and Ngauruhoe volcanoes, *J. Volcanol. Geotherm. Res.* **9,** 293–309.

Legrand, D., A. Calahorrano, B. Gillier, L. Rivera, M. Ruiz, D. Villagomez, H. Yepes (2002). Stress tensor analysis of the 1998–1999 tectonic swarm of northern Quito related to the volcanic swarm of Guagua Pichincha volcano, Ecuador, *Tectonophysics* **344,** 15–36.

Lu, Z., and M. Wyss (1996). Segmentation of the Aleutian plate boundary derived from stress direction estimates based on fault plane solutions, *J. Geophys. Res.* **101,** 803–816.

Lu, Z., R. Flatland, M. Wyss, S. Li, J. Eichelberger, K. Dean, and J. Freymueller (1997). Deformation of New Trident volcano measured by ERS-1 SAR interferometry, Katmai National Park, Alaska, *Geophys. Res. Lett.* **24,** 695–698.

Malone, S. D. (1983). Volcanic earthquakes: examples from Mount St. Helens, in *Earthquakes: Observations, Theory and Interpretation*, H. Kanamori and E. Bosch (Editors), Societa Italiana di Fisica, Bologna, 436–455.

Matumoto, T. (1971). Seismic body waves observed in the vicinity of Mount Katmai, Alaska, and evidence for the existence of molten chambers, *Geol. Soc. Am. Bull.* **82,** 2905–2920.

Matumoto, T., and P. L. Ward (1967). Microearthquake study of Mount Katmai and vicinity, Alaska, *J. Geophys. Res.* **72,** 2557–2568.

Miller, A. D., G. R. Foulger, and B. R. Julian (1998). Non-double-couple earthquakes. II. Observations, *Rev. Geophys.* **36,** 551–568.

Mogi, K. (1962). Magnitude-frequency relation for elastic shocks accompanying fractures of various materials and some related problems in earthquakes, *Bull. Earthquake Res. Inst.* **40,** 831–853.

Moran, S. C. (1994). Seismicity at Mount St. Helens, 1987–1992: evidence for repressurization of an active magmatic system, *J. Geophys. Res.* **99,** 4341–4354.

Moran, S. C., J. M. Lees, and S. D. Malone (1999). P wave crustal velocity structure in the greater Mount Rainier area from local earthquake tomography, *J. Geophys. Res.* **104,** 10,775–10,786.

Moran, S. C., J. A. Power, and S. D. Stihler (2001). Volcanic earthquake triggering by dynamic stresses associated with nearby tectonic earthquakes: constraints from the Katmai Group volcanoes, Alaska, *EOS* **82,** Fall Meeting Supplement, F837.

Moran, S. C., D. R. Zimbelman, and S. D. Malone (2000). A model for the magmatic-hydrothermal system at Mount Rainier, Washington, from seismic and geochemical observations, *Bull. Volcanol.* **61,** 425–436.

Mori, J., R. A. White, D. H. Harlow, P. Okubo, J. A. Power, R. P. Hoblitt, E. P. Laguerta, A. Lanuza, and B. C. Bautista (1996). Volcanic earthquakes following the 1991 climactic eruptions of Mount Pinatubo: strong seismicity during a waning eruption, in *Fire and Mud: Eruptions and Lahars of Mount Pinatubo, Philippines*, C. G. Newhall and R. S. Punongbayan (Editors), Univ. of Wash. Pr, Seattle, 339–350.

Motyka, R. J., S. A. Liss, C. J. Nye, and M. A. Moorman (1993). Geothermal resources of the Aleutian Arc, *Alaska Div. of Geol. and Geophys. Surv. Profess. Rept. PR-114.*

Nakamura, K., G. Plafker, K. H. Jacob, and J. N. Davies (1980). A tectonic stress trajectory map of Alaska using information from volcanoes and faults, *Earthquake Res. Inst. Bull.* **55,** 8910.

Parker, R. L., and M. K. McNutt (1980). Statistics for the one norm misfit measure, *J. Geophys. Res.* **85,** 4429–4430.

Power, J. A., S. C. Moran, S. R. McNutt, S. D. Stihler, and J. J. Sanchez (2001). Seismic response of the Katmai volcanoes to the 6 December 1999 magnitude 7.0 Karluk Lake earthquake, Alaska, *Bull. Seism. Soc. Am.* **91,** 57–63.

Pulpan, H., and F. Kienle (1979). Western Gulf of Alaska seismic risk, *Proc. of the 11th Annual Offshore Technology Conf.*, Houston, Texas **4,** 2209–2218.

Reasenberg, P. A., and D. Oppenheimer (1985). Fortran computer programs for calculating and displaying earthquake fault plane solutions, *U.S. Geol. Surv. Open-File Rept. 85-379*.

Roman, D. C., J. A. Power, S. C. Moran, K. V. Cashman, and S. D. Stihler (2001). Unrest at Iliamna volcano, Alaska, in 1996—Evidence for a magmatic intrusion? (abstract), *EOS* **82,** 1329.

Saltus, R. W. (1992). Principal facts for 63 gravity stations in the vicinity of Katmai National Park, Alaska, *U.S. Geol. Surv. Open-File Rept. 92-310*.

Saltus, R. W., D. Stone, J. Kienle, and A. M. Goodliffe (1991). New gravity data at Katmai National Park, Alaska, suggest a magma body analogous to that at the Geysers–Clear Lake Region, California (abstract), *EOS* **72,** 429.

Sanchez, J. J. (2000). Inversion of focal mechanism data for the directions of stress near Redoubt volcano, Alaska, *Master's Thesis*, University of Alaska, Fairbanks.

Scholz, C. H. (1968). The frequency-magnitude relation of microfracturing in rock and its relation to earthquakes, *Bull. Seism. Soc. Am.* **58,** 399–415.

Terzaghi, K., and F. E. Richart (1952). Stress in rock about cavities, *Geotechnique* **3,** 57–90.

Wallmann, P. C., D. D. Pollard, W. Hildreth, and J. C. Eichelberger (1990). New structural limits on magma chamber locations at the Valley of Ten Thousand Smokes, Katmai National Park, Alaska, *Geology* **18,** 1240–1243.

Waldhauser, F., and W. L. Ellsworth (2000). A double-difference earthquake location algorithm: method and application to the northern Hayward Fault, California, *Bull. Seism. Soc. Am.* **90,** 1353–1368.

Ward, P. L., A. M. Pitt, and E. Endo (1991). Seismic evidence for magma in the vicinity of Mt. Katmai, Alaska, *Geophys. Res. Lett.* **18,** 1537–1540.

Warren, N. W., and G. V. Latham (1970). An experimental study of thermally induced microfracturing and its relation to volcanic seismicity, *J. Geophys. Res.* **75,** 4455–4464.

Wessel, P., and W. H. F. Smith (1991). Free software helps maps and display data, EOS **72,** 441, 445–446.

Wood, C. A., and J. Kienle (Editors) (1990). *Volcanoes of North America*, Cambridge U Press, New York.

Wyss, M. (1973). Towards a physical understanding of the earthquake frequency distribution, *Geophys. J. R. Astr. Soc.* **31,** 341–359.

Wyss, M., B. Liang, W. R. Tanigawa, and W. Xiaoping (1992). Comparison of orientations of stress and strain tensor based on fault plane solutions in Kaoiki, Hawaii, *J. Geophys. Res.* **97,** 4769–4790.

Zoback, M. (1992). First- and second-order patterns of stress in the lithosphere: the world stress map project, *J. Geophys. Res.* **97,** 11,703–11,728.

Seth C. Moran
U.S. Geological Survey
Alaska Volcano Observatory
4200 University Dr.
Anchorage, Alaska 99508
scmoran@usgs.gov

Manuscript received 25 April 2002.